Hypersonic Laminar Instability on Round Cones Near Zero Angle of Attack

Steven P. Schneider*
School of Aeronautics and Astronautics
Purdue University
West Lafayette, IN 47907-1282

Abstract

Reliable predictions for hypersonic laminar-turbulent transition will have to be based on simulation of the transition mechanisms. Accurate simulation of the second-mode instability-wave growth on a round cone at zero angle of attack would be a significant step toward this goal. Hypersonic stability experiments in this geometry are reviewed, and three are selected. Extensive and previously unpublished data from Stetson's sharp and blunt cone experiments are reported. Approximate computations were carried out using inviscid-boundary-layer and e^N methods. The experimental results are compared to previous high-accuracy computations and to the present approximate computations. Quantitative agreement is at present insufficient for reliable e^N predictions. The difficulties with both experiment and computation are described.

Introduction

General Issues

Laminar-turbulent transition in high-speed boundary layers is important for prediction and control of heat transfer, skin friction, and other boundary layer properties. However, the mechanisms leading to transition are still poorly understood, even in low-noise environments [1]. Applications hindered by this lack of understanding include reusable launch vehicles, high-speed interceptor missiles, hypersonic cruise vehicles, reentry vehicles (RV's) [2], and discrimination among incoming RV's [3].

The transition process is initiated through the growth and development of disturbances originating on the body or in the freestream [4]. The receptivity mechanisms by which the disturbances enter a boundary layer are influenced by roughness, waviness, bluntness, curvature, Mach number, and so on. The growth of the disturbances is determined by the instabilities of the boundary layer. These instabilities are in turn affected by all the factors determining the mean boundary layer flow, including Mach number, transverse and streamwise curvature, pressure gradient, and temperature [1]. Relevant instabilities include the concave-wall Görtler instability [5], the first and second mode TS-like instability waves described by Mack [6], and the 3D crossflow instability [7]. The first appearance of turbulence is associated with the breakdown of the instability waves, which is determined by various secondary instabilities [8]. Local spots of turbulence grow downstream through an intermittently-turbulent region whose length is dependent on the local flow conditions and on the rate at which spots are generated [9].

In view of the dozens of parameters influencing transition, classical attempts to correlate the general transition 'point' with one or two parameters such as Reynolds number and Mach number can only work for cases that are similar to those previously tested. For general flight data, the scatter is large (e.g., Ref. [10]). Transition-estimation methods that are reliable for a broad range of conditions will need to be based on an understanding of the physical mechanisms involved.

The simplest and best developed of the mechanism-based methods are the e^N methods, which attempt to correlate transition with the integrated growth of the linear instability waves. Although these methods neglect receptivity and all nonlinear effects, such as wave interactions, nonlinear breakdown effects, roughness, and so on, they have shown promising agreement with experiment

*Associate Professor. Associate Fellow, AIAA.

Report Documentation Page

Form Approved
OMB No. 0704-0188

1. REPORT DATE	2. REPORT TYPE	3. DATES COVERED
01 JAN 2006	**N/A**	**-**

4. TITLE AND SUBTITLE	5a. CONTRACT NUMBER
Hypersonic Laminar Instability on Round Cones Near Zero Angle of Attack	5b. GRANT NUMBER
	5c. PROGRAM ELEMENT NUMBER
6. AUTHOR(S)	5d. PROJECT NUMBER
	5e. TASK NUMBER
	5f. WORK UNIT NUMBER
7. PERFORMING ORGANIZATION NAME(S) AND ADDRESS(ES) **School of Aeronautics and Astronautics Purdue University West Lafayette, IN 47907-1282**	8. PERFORMING ORGANIZATION REPORT NUMBER
9. SPONSORING/MONITORING AGENCY NAME(S) AND ADDRESS(ES)	10. SPONSOR/MONITOR'S ACRONYM(S)
	11. SPONSOR/MONITOR'S REPORT NUMBER(S)

12. DISTRIBUTION/AVAILABILITY STATEMENT
Approved for public release, distribution unlimited

13. SUPPLEMENTARY NOTES
See also ADM001860, Technologies for Propelled Hypersonic Flight (Technologies des vols hypersoniques propulses)., The original document contains color images.

14. ABSTRACT

15. SUBJECT TERMS

16. SECURITY CLASSIFICATION OF:			17. LIMITATION OF ABSTRACT	18. NUMBER OF PAGES	19a. NAME OF RESPONSIBLE PERSON
a. REPORT	b. ABSTRACT	c. THIS PAGE			
unclassified	**unclassified**	**unclassified**	**UU**	**24**	

Standard Form 298 (Rev. 8-98)
Prescribed by ANSI Std Z39-18

[1]. Agreement is fairly good for a variety of conditions where the environmental noise is generally low [11]. However, the accuracy of many high-speed e^N computations remains uncertain, for it is often not clear whether bluntness effects, wall temperature distributions, and so on were handled with sufficient accuracy [12]. Highly accurate mean-flow profiles are essential, since the stability equations are very sensitive to the second derivatives of these profiles. Although wave interaction effects and 3D effects can sometimes be handled with correlations [13], e^N methods are only an intermediate step along the way to reliable mechanism-based methods.

Direct simulations of transition [14] and the recently developed Parabolized Stability Equations (PSE) [15] have in some ways advanced theoretical-numerical work far ahead of the experimental database. The numerical work is not yet able to include complex effects such as roughness, waviness, internal shocks, and most bypasses. Three-dimensional mean flows and their instabilities are only beginning to be treated correctly from first principles [16]. The simulation of bluntness effects [17] and chemistry effects [18, 19] from first principles is only beginning. When the numerics are based on the correct physical mechanisms, however, they can provide much more detail regarding the transition process. Experimental work that describes not only the location of transition but also the mechanisms involved is needed in order to improve these modern theories. The key mechanisms need to be identified, in part through experimental work, and the key numerical results need to be validated experimentally.

Unfortunately, most of the ground-test data are ambiguous, due to operation in high-noise conventional wind tunnels and shock tunnels, with disturbance levels much higher than in flight [20]. The mechanisms of transition operational in small-disturbance environments can be changed or bypassed altogether in high-noise environments [21].

Transition on Reentry Vehicles

Laminar-turbulent transition is the dominant error source in aerothermal heating analyses of ballistic reentry vehicles. This is shown, for example, in Fig. 8 of Ref. [22], which presents computations and measurements of the surface heat transfer during the Reentry-F test. Agreement is good for both the laminar and turbulent regions, once the transition location is known. Harris Hamilton from NASA Langley says that typical accuracies are 20-25% for the turbulent boundary layer, and 15-20% for the laminar layer. The largest uncertainty is due to transition, which causes a large increase in the heat transfer rates (private communication, March 1999). Similar results are reported in Ref. [23]. Ref. [10] shows typical empirical correlations such as Re_θ/M_e, around which the data scatter by as much as a factor of 3.

Real ballistic RV's are ablating, rough, and at non-zero angle of attack. Ground-test measurements of transition will not be able to simultaneously simulate all the characteristics of the high-enthalpy flight environment; thus, ground-based experiments must discover and document the transition mechanisms, in order to develop and validate computational models which are then extended to flight conditions [24]. For ground-test measurements of stability, a smooth-wall perfect-gas cold-flow round cone with small bluntness is a reasonable first approximation. Measurements of the instability waves (or transition mechanisms) are needed under these conditions, for comparison to computation. A number of stability experiments have been carried out for this case. Although all contain significant flaws, a detailed reanalysis of this data is being carried out for NATO RTO Working Group 10 (WG 10). The present work summarizes this reanalysis, and presents comparisons to computations reported in the literature, and to limited-accuracy e^N computations carried out by the author.

Review of Stability Experiments

A necessary step in the further development of mechanism-based methods is accurate computation of the actual instability-wave growth. At high speeds, this is a major challenge. At low speeds, such computations were slow to become validated (e.g., Ref. [25]); this validation is more critical at high speeds, where there are many more physical factors whose influence must be properly taken into account. However, even in noisy conventional tunnels, there are few measurements of the instability mechanisms causing transition. Of these instability measurements, few have been carried out with calibrated instruments and well-documented conditions, so that a fairly reliable comparison to computations can be carried out. Rather, existing stability experiments have mainly served to *discover* the stability phenomena, confirm the fundamental aspects of the theoretical predictions, and supply preliminary quantitative information. While such experiments have been an important step forward, the requirements for *code validation* experiments are much more stringent (e.g. Refs. [26] and [27]). Even

for the surface pressure distribution under cold-flow conditions, accurate validated results remain to be obtained [28].

The transition members of WG 10 felt that the following elements should be present in code-validation experiments for hypersonic transition:

1. Detailed and reliable measurements of the transition mechanisms.

2. Accurate knowledge of the mean flow. Repeated checks of boundary layer symmetry, instrumentation calibrations, tunnel flow nonuniformity effects, repeatability, etc. Accurate agreement with computation of mean flow. This requires repeated tunnel entries and cooperation between experiments and computations.

3. Linear instability comparisons require calibrated measurements of the fluctuations at a known position in the eigenfunction. It seems possible that these might be carried out in conventional tunnels using ensemble averaging of controlled disturbances.

4. Nonlinear secondary breakdown effects are dependent on small fluctuations combining with the primary instability. It seems doubtful that these can be repeatably and successfully studied except in quiet tunnels, since even controlled secondary disturbances may be swamped by tunnel noise. For similar reasons, receptivity experiments may also require quiet flow.

These specifications are updated from Ref. [29], which gives additional suggestions, and shows the long-term importance of a coordinated approach.

Unfortunately, these specifications are extremely difficult to meet at hypersonic speeds. Although new experimental efforts are underway at Purdue and at ITAM, Novosibirsk, Russia, all existing data fall short. Despite these shortcomings, it seemed valuable to assess the best existing datasets in detail, as both a determination of the state of the art, and as a means of finding the improvements that are needed. Three datasets were identified for further analysis. New experimental measurements are presently being obtained at ITAM, Novosibirsk, Russia [30]; these are not complete, and have not yet been examined in detail.

While the following three datasets all contain significant flaws and limitations, they are the best presently available, in the opinion of the team. Accurate computation of the wave growth and eigenfunctions for these cases would be a significant step towards the further development of mechanism-based methods. Comparisons between the experiments and the results of multiple independent computations would shed light on the strong and weak elements in all, and aid in planning new work.

Because of the limited resources presently available, attention is focused on axisymmetric geometries. The computational resources required are much less than in the 3D case. All of the datasets are for cold hypersonic flow without chemistry, because detailed measurements of the mechanisms of high-enthalpy hypersonic transition do not exist. Although the data shown below are primarily measurements of the cold-flow second-mode instability, other mechanisms do of course remain important.

Present Computations Using Approximate Methods

Several of the experimental flows were computed by the author using fairly elementary methods that are commonly available to nonspecialists. The inviscid axisymmetric flows were computed by Sandia National Labs and provided by Dr. Dave Kuntz. The `2IT` code was used to compute the inviscid nosetip flow [31]. This code solves the unsteady Euler equations using a time-dependent, finite-difference technique, with the cylindrical flowfield mapped into a computational domain. The technique is shock-fitting in nature, with the characteristic compatibility relations invoked at the bow shock and impermeable surface boundaries. MacCormack's explicit scheme is used to integrate the governing equations, producing a solution technique which is second order in both time and space. The solution is converged in time to produce both a steady-state flowfield solution on the spherical nosetip and an initial data plane for the afterbody code.

The afterbody flowfield, surface pressure, and shock shape, were solved with the SANDIAC code [32], an extension of the GE-3IS-SCM/ACM code [33, 34, 35]. This code is also shock fitting, and solves the steady, two or three dimensional Euler and conservation of energy equations. A cylindrical based coordinate system transformed to a computational space is used to allow computations on an equally spaced grid. The difference equations are integrated by the Beam-Warming modified upwind MacCormack scheme [36] using the Van Leer flux vector splitting scheme [37]. Characteristic compatibility relations are also used to compute the surface pressure.

The shock shape and surface-pressure distribution were provided to the Harris finite-difference code [38]. This code is second-order accurate, and can include a first-order correction for variable entropy. In the first iteration, the boundary layer is computed as if the stagnation streamline wetted the entire body. Using conservation of mass, the code then traces streamlines upstream from where they enter the boundary layer to where they pass through the shock. The shock angle at this point is used to compute the entropy and total pressure on the streamline, downstream. In the second iteration, this variable entropy is used in a new edge condition, to recompute the boundary layer. Although it is well known that this will not give the correct boundary-layer profile in the outer region (Julius Harris, private communication, Sept. 1991), this code is fairly easy to use and readily available. This code runs in a few seconds on a 400MHz Pentium II.

Unfortunately, the computations based on the first-order Harris code showed poor agreement with the Stetson blunt-cone experiments, as will be discussed. Further computations are to be carried out using a viscous-shock-layer (VSL) code, which is also readily available [39, 40]. This method solves the inviscid and viscous flows in a coupled way that is substantially more accurate, while remaining substantially simpler and faster than existing Navier-Stokes or Parabolized Navier-Stokes codes. However, VSL results have not yet been obtained, due to the time required to learn the use of the code. This VSL code also runs in a few seconds on a 400MHz Pentium II.

The boundary-layer profiles from the Harris code were then supplied to the e^{MALIK} code for computation of instability waves [41, 42]. This code solves for compressible parallel-flow linear instability, including transverse curvature effects. An automated system that links these codes was previously developed (e.g., Ref. [43]). Boundary-layer profiles from the VSL code have not yet been used for stability analysis. The stability code can run several frequencies along the length of a cone in a few hours on the back processor of a dual-Pentium-II 400MHz PC. This speed is sufficient for design purposes, if a suitably validated code can be developed.

Sharp Cone at Mach 8

General Information

Stetson et al. carried out calibrated measurements of instability wave growth on several conical models in AEDC Tunnel B at Mach 8, during the late 1970's and early 1980's [44, 45]. Detailed hot-wire measurements were carried out in this expensive production tunnel by J. Donaldson, under the direction of K. Stetson [46, 47]. Both are now retired, although Stetson is still available for discussions. The experiments were focused on the hypersonic second-mode instability, which is likely to be dominant on smooth convex nearly-symmetric geometries with small crossflow. Although these are conventional-tunnel measurements with high ambient noise, the good-quality detailed measurements appear to deserve further computational comparisons. Detailed measurements of the disturbances in this tunnel are available [48].

The model was a 7-degree half-angle cone with a 40-inch (1.016-m) length and a sharp 0.0015-inch (38 micron) nose radius. The cone angle of attack was zero, to within the accuracy with which this could be set and measured. The model was in thermal equilibrium, but heat conduction within the model was not negligible.

Most of the measurements were carried out at a freestream Mach number of 7.95, with a total pressure of 225 psia (1.55 MPa) and a total temperature of 1310 R (728 K). Additional data were recorded at a lower total pressure, to determine the neutral-instability region; while this data could be used for linear-amplification analysis, the amount of data is limited (see Fig. 24 of Ref. [45]). Data was also acquired at a higher pressure, to record data into transition onset. Thus, transition-onset data should be available.

Measurements were carried out with surface pressure taps (24) and thermocouples (32). Mean-flow profiles were obtained using pitot-pressure and total temperature probes. Instability-wave spectra were obtained using calibrated constant-current hot-wire anemometry. Hot-wire measurements were recorded at one-inch (2.54-cm) intervals between 10 and 37 inches (25.4 and 94.0 cm), using a single hot-wire with a single calibration. Since the measurements were obtained only along a single ray, and only at the height above the wall where the broadband amplitude is a maximum, Stetson has expressed concern about three-dimensional effects (pp. 14-15 of Ref. [45]).

Growth of first and second-mode instability waves was observed under cold-flow conditions. The second-mode instability was dominant. Second-harmonic amplification was observed downstream, a good indication of nonlinear effects. A comparison of the second-harmonic amplification rate to a nonlinear computation would be interesting.

Although Stetson [44] published a summary of these experiments, extensive tabulated data for the mean flow remained unpublished, along with extensive tabulations of the instability spectra for both uncalibrated and calibrated fluctuations. These tables were provided courtesy of Roger Kimmel and have been entered into electronic form and posted on the WG-10 website. Many detailed measurements are here reported for the first time.

The amplification rates reported by Stetson et al. [44] were obtained by curve-fitting and differentiating the experimental spectral-amplitude data. Although most of the past comparisons to computation made use of these amplification rates, differentiation of experimental data is a notoriously uncertain process which can introduce substantial errors. It is recommended that future comparisons should instead be made by integrating the computed amplification rates and comparing amplitude ratios between computation and experiment. This more-accurate process is now possible, due to the availability of the tabulated spectral amplitudes.

Previous Computational Comparisons

Mack carried out the first set of detailed comparisons to this experiment [49, 50]. Three methods were used to obtain the mean-flow profiles: 1) transformed flat-plate profiles, 2) cone profiles from the axisymmetric boundary-layer equations, without the transverse curvature term, and 3) like (2), but with the transverse curvature term. The wall was assumed adiabatic. Preliminary computations including the effect of the experimental surface-temperature gradient are reported to show only minor effects. The stability was analyzed using parallel-flow linear instability theory. Locally planar flow is assumed in the stability analysis. Mack uses the Sutherland viscosity law down to 110.4K, and a linear law below this (see also p. 57 of Ref. [6], where this law is stated without justification).

The effect of total temperature was found to be significant. The effect of transverse curvature was small (7% for one amplification rate). At $R = 1730$, the measured frequency of the maximum amplification rate was less than 10% higher than the computation. However, the computed amplification rate is about 50% higher than the measured value. Here, $R = \sqrt{Re_{xe}}$, the square root of the usual length Reynolds number, $Re_{xe} = U_e x/\nu_e$. Fig. 19 in Ref. [44] shows that the experimental amplification-rate curve at this location is in general agreement with earlier measurements by Kendall [51] and Demetriades [52].

Fig. 5 in Ref. [50] shows that the computed maximum amplification rate is close to the measured value for $1200 < R < 1400$, but the measured value increasingly drops below the computed value for $R > 1400$. Fig. 21 in Ref. [45] shows that higher harmonics also become significant for $R > 1400$. Stetson [45] concludes that nonlinear effects become significant for $R > 1400$, making comparisons to a linear amplification rate inappropriate there. This is a very important point, for most later computations follow Mack in comparing to the experiment at $R \simeq 1732$. Fig. 18 in Ref. [49] shows an N-factor comparison that makes the same point – the experimental amplification rates are lower than the computed values, particularly above $R \simeq 1800$ where the experimental amplitudes actually decrease. Mack suggests that this is due to nonlinear effects or to the start of transition.

Mack also suggests that the experimental amplification rate may be lower because a pure 2D normal mode is not what is actually being measured. He points out that different frequencies may have their maximum response at different boundary-layer heights, so a Fourier analysis of the signal at the height where the broadband amplitude is a maximum does not necessarily determine the single-mode amplification rates.

Chang et al. [53] show one figure suggesting that a sharp-cone PNS solution can achieve better agreement at $R \simeq 1732$, but few details are given in the paper. Their linear-stability equations allow for shock motion. A similar comparison at $R \simeq 1730$ is shown in Fig. 4 of Ref. [54]; the computational growth rates are about 20% above the experimental values. Few details are again given.

Chang et al. [55] performed linear and nonlinear computations using PSE methods. The mean flow appears to be obtained using the Mangler transformation from the flat plate solution, but the details are sketchy. Chang et al. also find poor agreement between linear-instability theory and Stetson's amplification rates at $R \simeq 1730$. Nonparallel effects result in an increase in the computed growth rates, making the agreement worse. However, if appropriate nonlinear effects are taken into account, fairly good agreement can be obtained (Figs. 9 and 13 in Ref. [55]). Chang et al. suggest that nonlinear effects become dominant at $R \simeq 1600$. Various assumptions have to be made regarding the amplitude of the particular waves that are included in the nonlinear computation, so the nonlinear computation can only suggest an explanation for the experiment, it cannot be validated by the experiment. The

linear-region data was not studied in detail, probably because Chang et al. did not have ready access to the detailed tabulated data.

A series of detailed computational comparisons has been carried out by Dallmann's group at DLR, Göttingen, Germany. Simen et al. shows comparisons carried using a thin-layer Navier-Stokes code, combined with local linear instability theory [56, 57, 58]. Fairly good agreement is obtained for the downstream mean profiles, and for the second-mode growth rates. However, these comparisons were later repeated by Kufner, using the same code [59, Section 6.2]. Kufner did not obtain the same good agreement, even when using Simen's grid. According to Stefan Hein (private communications, October-December 2000) and Ref. [60], Kufner believed that Simen's good agreement was due to insufficient convergence, insufficient grid resolution, insufficient clustering of the grid near the shock, and a fortuitous value of the entropy-fix parameter that is needed to stabilize the solution. Kufner obtained fully converged grid-independent solutions that were independent of the entropy-fix parameter, over a certain range. These solutions resulted in amplification rates that were in general agreement with the other computations, and that disagree with the experimental data. Since Esfahanian also obtained fortuitous agreement when using Simen's grid (Stefan Hein, private communication, October 2000), it appears that Simen's good agreement was a misleading coincidence.

In summary, at the present time it appears that Stetson's sharp-cone experiments show waves that rise above the background noise for $R \simeq 1200$, grow linearly only in the short region to $R \simeq 1400$, and become nonlinear downstream. Most detailed comparisons to linear instability have mistakenly been carried out downstream, where the growth is actually nonlinear, and comparisons to the $R \simeq 1730$ growth rates therefore show poor quantitative agreement. Now that the detailed tabulated data are available, new comparisons should be performed for the linear instability amplification.

Mean Flow Comparisons

Fig. 1 shows the wall temperature distributions measured on the sharp cone, at the time of various mean-profile measurement runs. The coordinate s is the arclength along the surface. The x locations in the legend are the axial locations of the respective mean-profile measurements, and T_w is the surface wall temperature. The forward portion of the model heats up with time, and the aft portion appears to

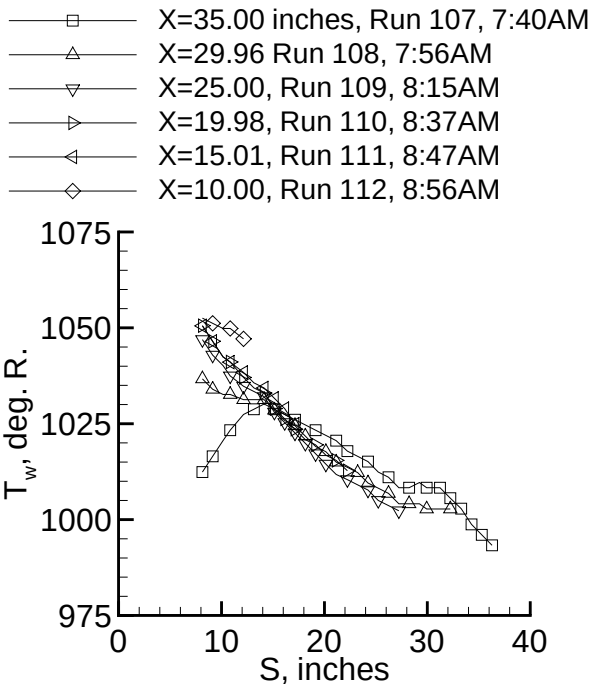

Figure 1: Wall Temperatures for Stetson Sharp Cone

cool slightly. The data do not agree with a simple analysis of the adiabatic wall temperature. The temperatures are the result of a complex heat balance in the thin-wall model, which incorporates a solid nosetip and a water-cooled sting support.

Fig. 2 and 3 show the tabulated sharp cone mean profiles. Both show overshoots near the edge of the boundary layer. While it is commonly accepted that the total temperature can overshoot near the boundary layer edge, the overshoot in the pitot profile is suspicious.

Fig. 4 shows a preliminary comparison to a simple computation. The comparison is shown for Run 107, at $P_t = 225.3$ psia, $T_t = 1364.4$R, and $M_\infty = 7.95$. Here, P_t and T_t are the total pressure and temperature in the stilling chamber, and M_∞ is the freestream Mach number in the test section. The measured pitot profiles are compared to boundary layer computations based on the Harris finite-difference code [38] and the Taylor-Maccoll solution. The computational profiles were reduced to pitot pressure using the Rayleigh pitot formula above Mach 1, and the subsonic isentropic formula below Mach 1. The streamwise distance $x = 35.0$ inches, and the arc length distance $s = 35.26$ in. or 2.939 ft. The isothermal computation assumed a 1000R wall temperature, which is near the mean

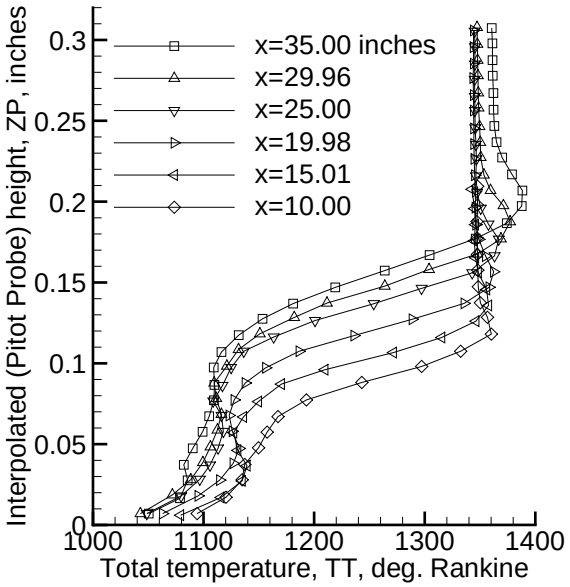

Figure 2: Mean Total Temp. Profiles for Stetson Sharp Cone

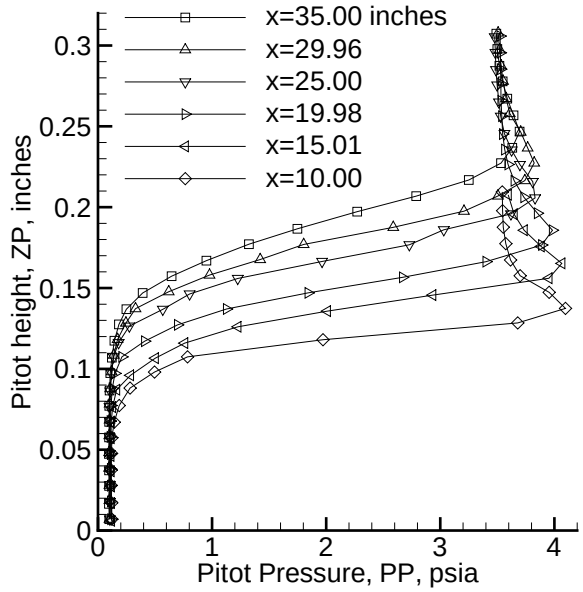

Figure 3: Mean Pitot Profiles for Stetson Sharp Cone

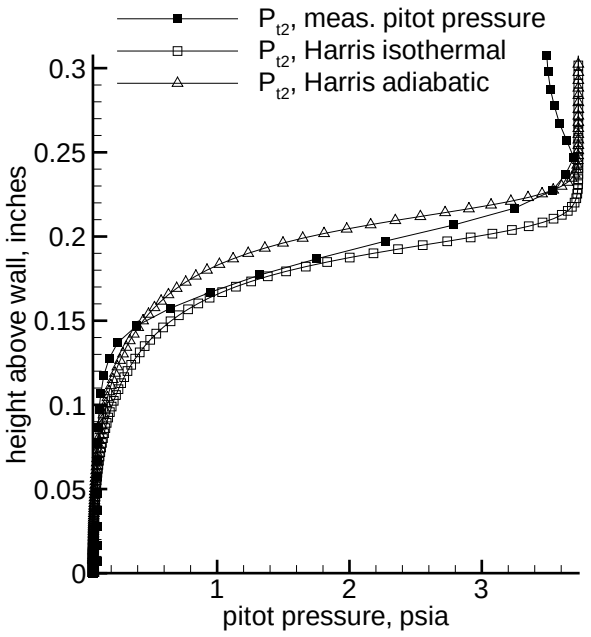

Figure 4: Pitot Profile Comparison for Stetson Sharp Cone

of the approximate measured wall temperature distribution. The adiabatic-wall computation results in wall temperatures $T_w \simeq 0.856T_t$, while the measured is $T_w \simeq 0.75T_t$.

The measurements show an overshoot in the pitot pressure which is not present in the computations. Such an overshoot has been observed before for blunt cones or at angle of attack [61], but the author is not aware of any reliable experimental data showing such an overshoot for a sharp cone at zero angle of attack. The obvious experimental causes might include small residual angles of attack or a bent cone tip. It was also thought possible that more sophisticated computational approaches may yield this overshoot. However, computations by Kufner using the thin-layer Navier-Stokes equations do not show this overshoot in the pitot profile (Fig. 5). These computations were carried out for the blunt-cone conditions of $T_t = 750$K, $T_\infty = 54.35$K, $M_\infty = 8.0$, $Re_\infty = 8.202 \times 10^6$/m, $\gamma = 1.4, R = 287.03$J/kg-K, and with a Sutherland constant of 110K. The Mack viscosity law is used [6, p. 57], resulting in a freestream Reynolds number that is 6% lower, as compared to the use of the Sutherland law even below 110K. The computational results were provided by Stefan Hein (private communication, April and October, 2000); see

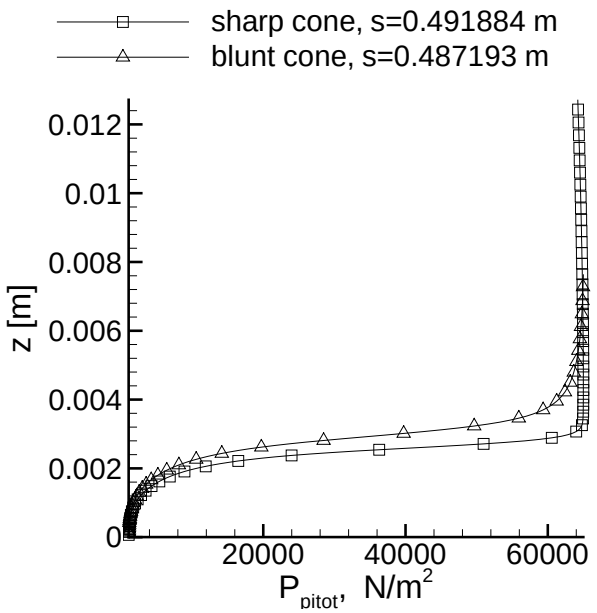

Figure 5: TLNS Pitot Profiles for Stetson Sharp and Blunt Cones at Blunt-Cone Flow Conditions, from Kufner via Hein

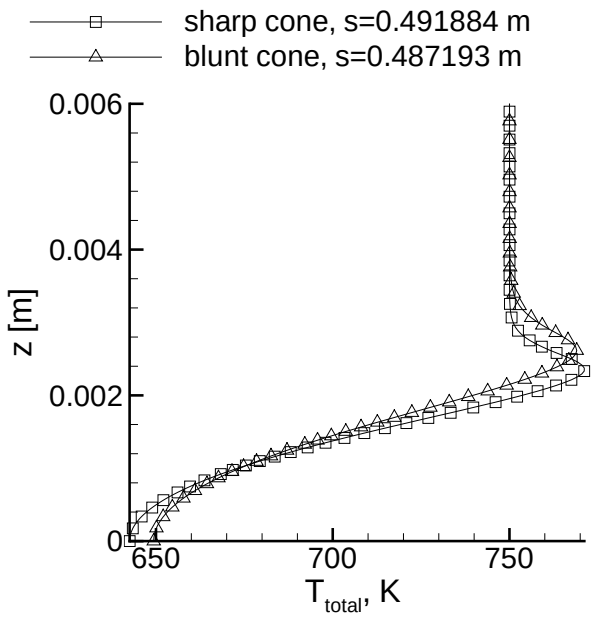

Figure 6: TLNS Total Temperature Profiles for Stetson Sharp and Blunt Cones at Blunt-Cone Flow Conditions, from Kufner via Hein

Ref. [62]. Neither the blunt cone nor the sharp cone (computed at the blunt-cone conditions, not the Stetson sharp-cone conditions) shows an overshoot in the pitot profile, although both show overshoots in the total-temperature profile (Fig. 6).

However, this pitot overshoot is similar to that observed by Kendall on a flat plate when insufficiently small pitot tubes were used. Measurements with smaller pitot tubes did not show an overshoot. The overshoot was then attributed by Kendall to probe interference [63]. A similar overshoot is observed in three references cited in Morkovin et al. [64]; Morkovin also explains the overshoot as probe interference. Since the overshoot decreases with downstream distance, as might be expected since the relative pitot-probe size decreases with increasing boundary-layer thickness, it seems likely that probe interference is the cause. This problem then casts doubt on all the mean-flow profiles.

Accurate mean-flow computations at the Stetson sharp-cone conditions were not available to this author, who is unaware of any definitive comparisons. However, the lack of a pitot-profile overshoot for a sharp cone was confirmed in unpublished Navier-Stokes computations by Manning et al. (private communication, July 2000; cp. Ref. [65]). The pitot-profile data thus appear to be contaminated with probe interference. Since the total-temperature profile data were obtained at the same time with the same probe assembly, they may also be contaminated; however, this remains to be shown by a comparison to accurate computations.

Instability-Wave Comparisons

The voltage spectra are shown in Fig. 7. Every other streamwise station is shown, to improve clarity. Since the measurements were made at the peak-amplitude height in the boundary layer, and since the sharp cone profiles should be self-similar, all measurements should be at the same mean-flow condition. A single hot-wire was used for all these measurements. Thus, all local calibrations should be identical, and ratios of voltage amplitude should be ratios of flowfield fluctuations. However, the data remain to be checked in detail. The variable `ZA` is the hot-wire height above the wall, in inches, and s is again the arc length.

The calibrated spectral amplitudes are also available and are published here for the first time in Figs. 8 and 9. These data were reduced in the early 1980's but the tabulated data were not published, as the qualitative features do not differ from the uncalibrated data. The printed tables were reduced to electronic form under the supervision of

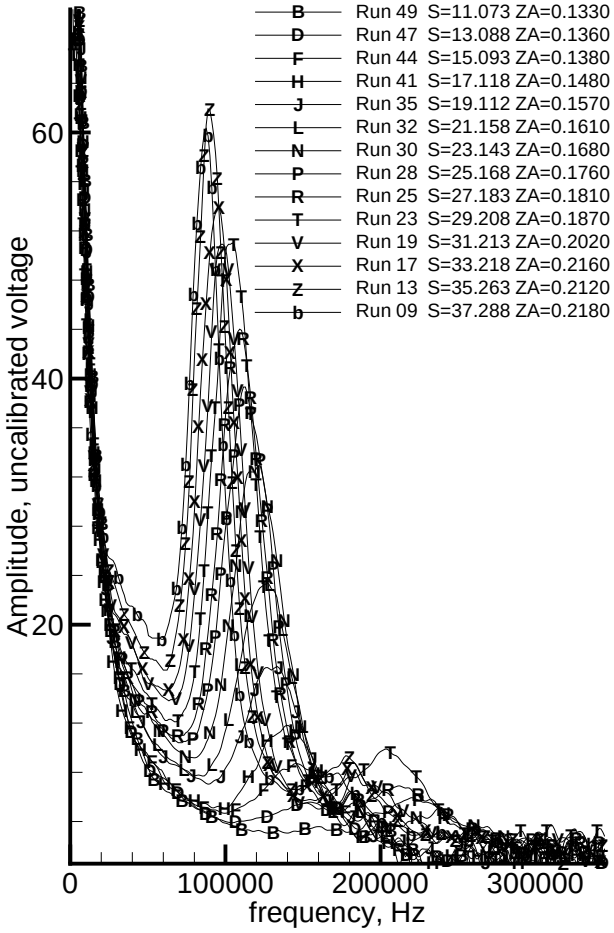

Figure 7: Voltage Spectra for Stetson Sharp Cone

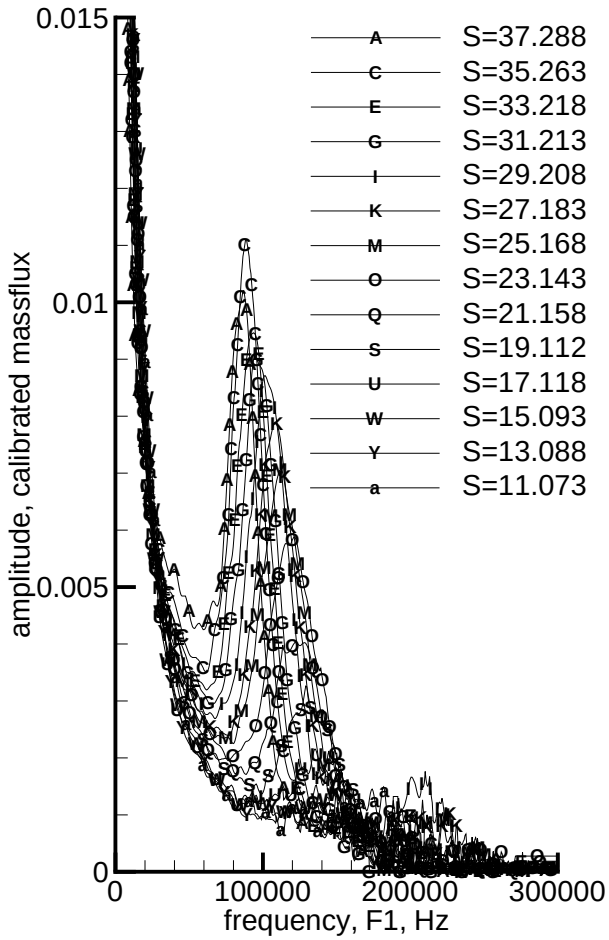

Figure 8: Massflux Spectra for Stetson Sharp Cone

Roger Kimmel of the Air Force Research Lab (private communication, October 2000). Figs. 8 and 9 show every other streamwise station, for improved clarity. The run numbers and measurement heights are the same as in the uncalibrated spectra. Both spectra are normalized by the mean values at the probe height. Tabulated data are available from Roger Kimmel or the author, or from the WG 10 website. Uncalibrated spectra from various freestream hot-wire measurements are also available in tabulated form.

The integrated growth of these waves was computed using the e^{Malik} code and compared to Mack's results. The internal similarity solver was used to obtain profiles for the e^{Malik} code. The Mack data were digitized from Fig. 6 in Ref. [49], since the original tabulated data are lost (Les Mack, private communication, July 2000). Figure 10 shows the results, for $T_t = 1310$R, $Re_e = 1.42 \times 10^6$/ft., $M_e = 6.8$,

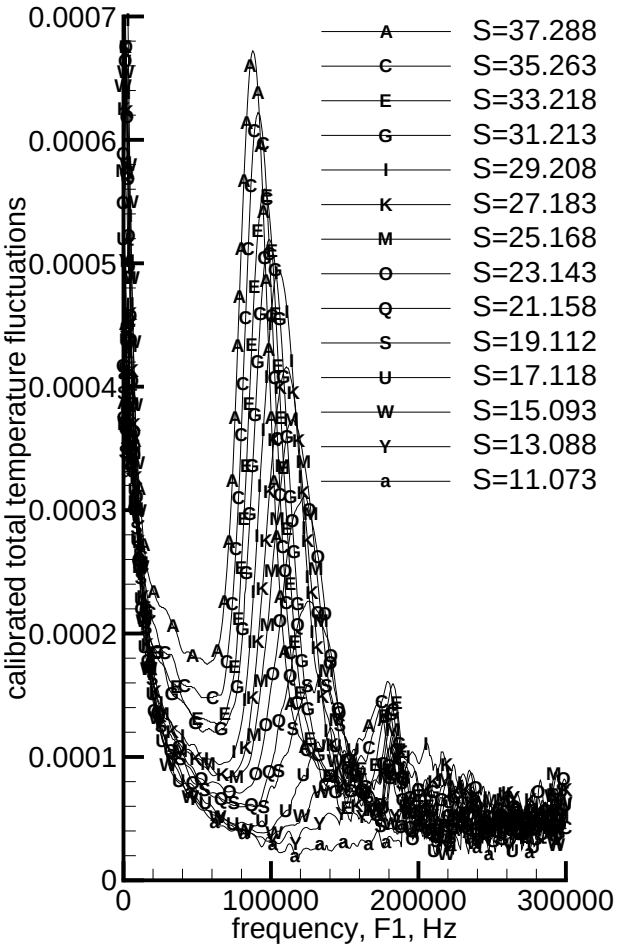

Figure 9: Total-Temperature Spectra for Stetson Sharp Cone

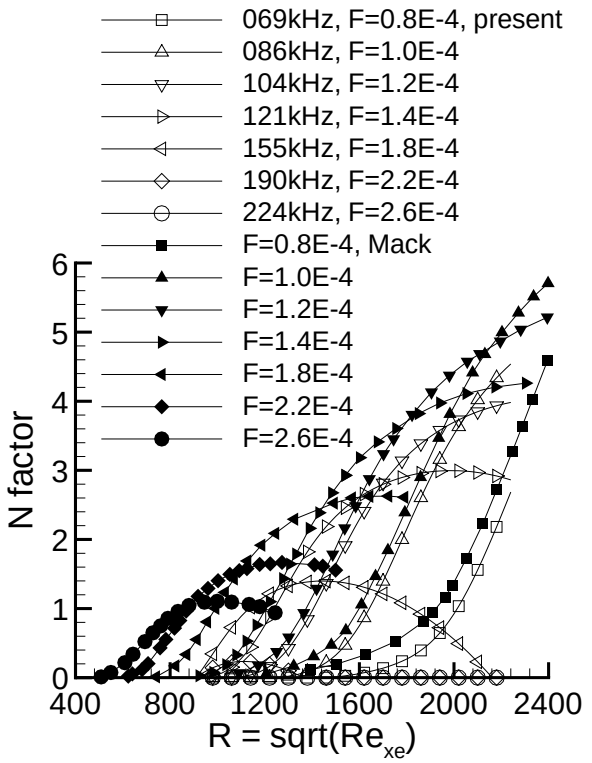

Figure 10: N-factor Computations for Stetson Sharp Cone; Profiles from Internal eMalik Solver

$Pr = 0.72$, and an adiabatic wall. Here, Re_e and M_e are the unit Reynolds number and Mach number at the boundary-layer edge, Pr is the Prandtl number, and F is the usual nondimensional frequency. Significant differences exist; in particular, the present computations find no instability at the higher frequencies, where Mack does find instability, and the N-factor for $F = 1.4 \times 10^{-4}$ at $R \simeq 2000$ differs by about 30%.

The cause of the difference is difficult to determine; detailed analysis by a computational expert is clearly required. Possibilities include differences in the numerical methods and the fluid property models, such as the heat-transfer coefficient, the viscosity coefficient, and the heat capacity. A different version of the e^{Malik} code was obtained from Roger Kimmel (private communication, July 2000); it gave results that differed substantially at high frequencies (e.g., from $N = 1.0$ to $N = 1.4$), when using the same input file and when executed on the same machine with the same compiler. The present version was earlier checked against Ref. [42]; see Ref. [66].

A set of computations was also carried out using the Taylor-Maccoll solution [67, Sec. 16.5], the Har-

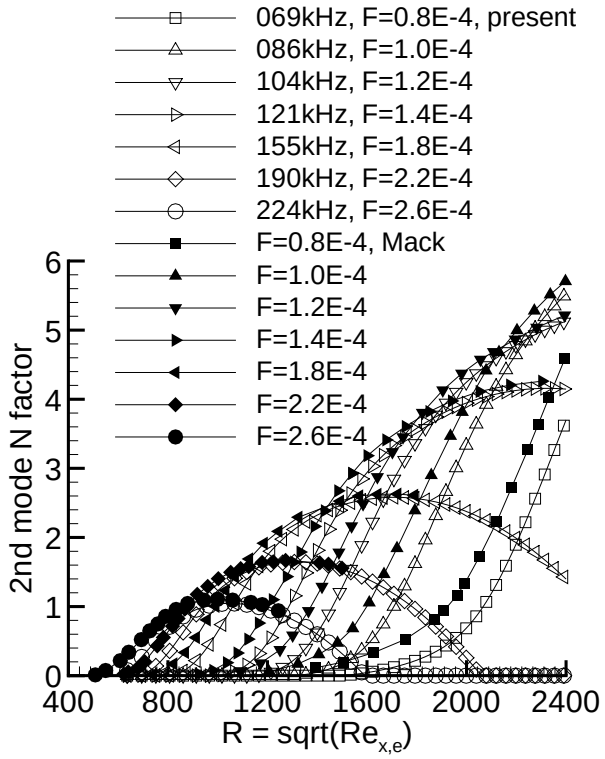

Figure 11: N-factor Computations for Stetson Sharp Cone; Profiles from Harris Boundary-Layer Code

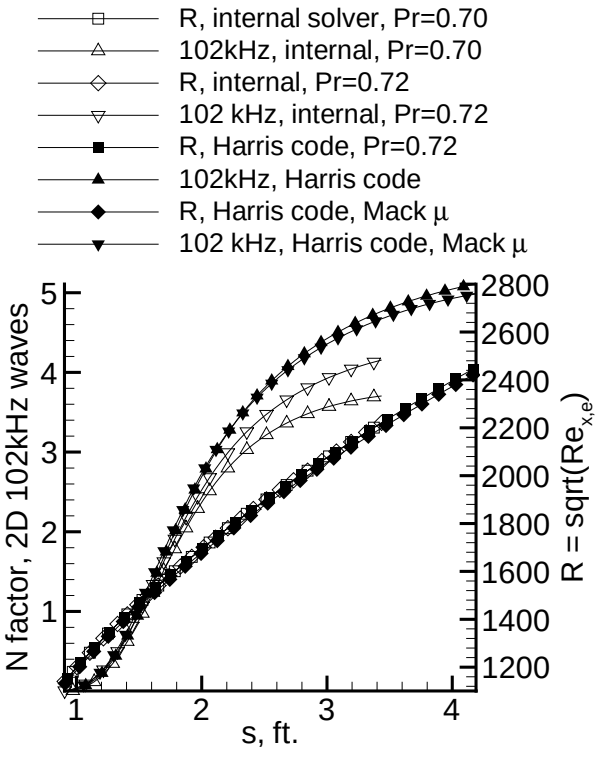

Figure 12: N-factor Computations for Stetson Sharp Cone; Four Methods for One Frequency

ris boundary-layer code, and the e^{Malik} code. Figure 11 shows another comparison to the Mack results, for $T_t = 1310$R, $P_t = 225$ psia, $Re_\infty = 1.0 \times 10^6$/ft., $M_\infty = 8.0$, $Pr = 0.72$, and an adiabatic wall. Here, the Harris code was modified to use the Mack-modified form of the Sutherland viscosity law. The comparison for the higher frequencies is better than that obtained using the internal e^{Malik} solver, due to small changes in the boundary-layer profiles and their derivatives (not shown). A doubling of the grid for the boundary-layer solution changed the present N-factor results by less than 0.5%.

Figure 12 shows a final comparison between computations. All are carried out at $T_t = 1364.4$R, $P_t = 225.3$ psia, $M_\infty = 7.95$, and for an adiabatic wall. A single frequency is computed, and both the N-factor and the value of R is shown vs. the streamwise distance s. For the first two sets, the profiles are obtained using the internal e^{Malik} similarity solver; for the last two, the profiles are obtained using the Taylor-Maccoll solution and the Harris boundary-layer code. The first pair of solutions differ in the value of the Prandtl number that is used. The first of the Harris-code solutions uses the Sutherland viscosity law, even below 110K; the second uses the Mack-modified Sutherland law. For the first 3 solutions, the value of R repeats almost exactly, as it should; for the last one, R differs somewhat due to the change in the freestream viscosity. For the two solutions using the internal similarity solver, the small change in Prandtl number changes the final N factor by some 12%. The larger of these two solutions is, in turn, about 10% below the Harris code solutions. The change in viscosity law (for the Harris code only) changes the N factor only slightly.

The best method of comparing to the experimental data is to integrate the computed amplification factors and compare the amplitude ratio to the experimental value. Since the experimental data are linear only to about $R = 1400$, and since the signal-to-noise ratio becomes substantial only at about $R = 1150$, the comparison was carried out from $R \simeq 1150$ to $R \simeq 1350$, as shown in Figure 13. The experimental voltage spectra were used for this plot. The computation was carried out using the Harris boundary-layer code, for $P_t = 225.3$ psia, $T_t = 1364.4$R, $M_\infty = 7.95$, using the Sutherland viscosity law, and with a 1000R isothermal wall tem-

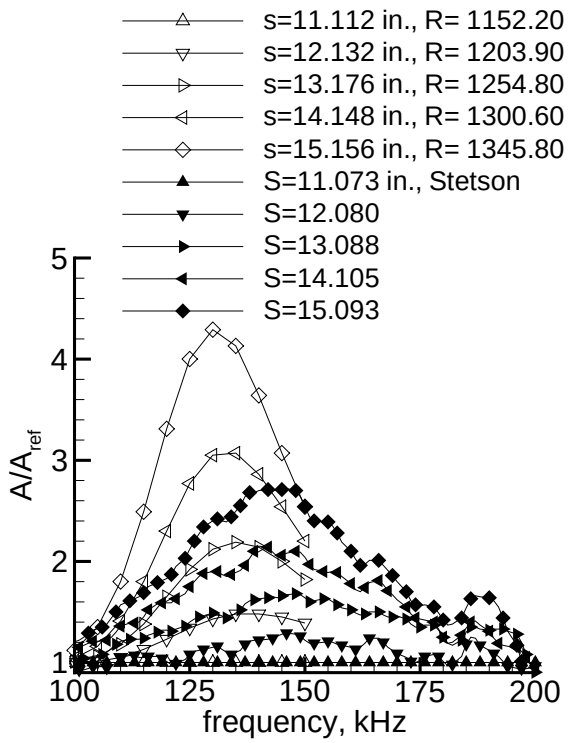

Figure 13: Amplitude-Ratio Comparisons for Stetson Sharp Cone

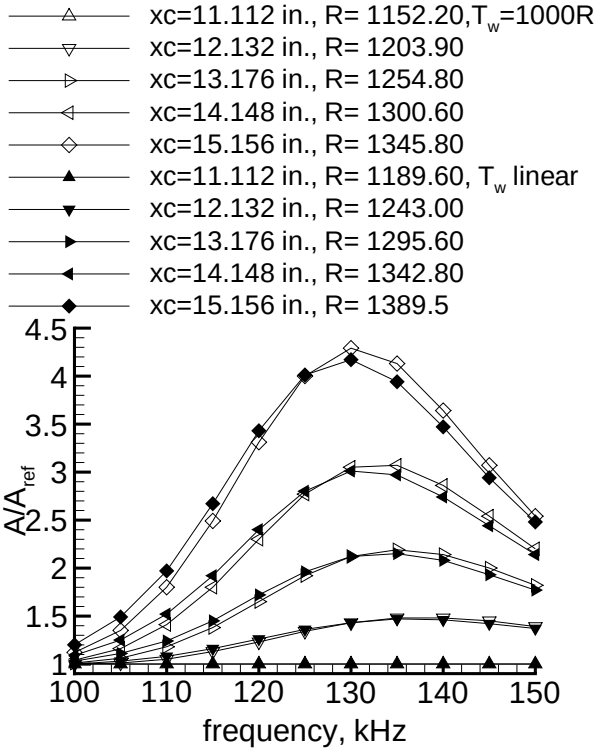

Figure 14: Amplitude-Ratio Comparisons for Stetson Sharp Cone: Two Wall Temperature Distributions

perature. For the computation, amplitude ratios are referenced to the values at $s = 11.112$ in., while the reference location for the experiments is $s = 11.073$ in., which is sufficiently close for this initial comparison. The experimental amplitude growth in this region is small, less than a factor of 3, which limits the accuracy of any comparisons. The early nonlinearity is probably due to the relatively large amplitude at which the signal becomes larger than the noise of the conventional wind tunnel. Compare Ref. [68], where growth of a factor of 2 is measured at a far lower Reynolds number under controlled quiet conditions. The computed maximum amplitude ratio is 60% larger than the experimental value, and the most amplified frequency in the computation is about 10% lower. The experimental peak N factor is about 1.0, while the computational value is about 1.5.

Figure 14 shows that the difference is probably not due to the effect of wall temperature distribution. Amplitude ratios are shown, as in Fig. 13, for the same flow conditions, again computed using the Harris boundary-layer code. The first set of amplitude ratios is obtained for a constant isothermal wall temperature of 1000R. The second set is for a linear variation of wall temperature from 1060R to 966R; this approximates the experimental distribution (Fig. 1). The reference location for both sets of amplitude ratios is $s = 11.112$ inches. The effect of the varying wall temperature is small.

Summary

It is remarkable that accurate agreement between experiment and computation remains to be obtained for the growth of second-mode waves on a round sharp cone at zero angle of attack. This shows the difficulty of accurately measuring and computing hypersonic instability. The experimental mean-profile data is clearly contaminated by probe interference, and cannot be used as a reliable check on the mean-profile computations. This means that it cannot be used to check angle of attack, mean flow nonuniformity, or other experimental error sources. The early nonlinearity observed in the experiments also suggests that comparisons of linear amplification must be carried out either with controlled disturbances or with a quiet tunnel, or both.

The computational results shown here highlight

the well-known sensitivity of instability computations to small errors in the numerics or the profiles. The difficulty no longer seems to be computer resources, but rather a robust and sufficiently accurate code. An accurate set of agreed-upon results should be readily available, for a mean flow and the instabilities, to allow benchmarking to be carried out. It is evident that this is needed even for an established code, when such a code is ported to a new location, user, or machine.

The poor agreement between the computation and experiment cannot be resolved until the computational and experimental methods are refined. The present experiments also suggest that nonlinear effects are a critical part of second-mode induced transition on sharp cones, since so much of the wave growth occurs nonlinearly. However, this remains to be confirmed by quiet-tunnel experiments.

Blunt Cone at Mach 8: Stetson et al.

General Information

In addition to the sharp cone measurements discussed above, Stetson et al. carried out additional calibrated measurements of instability wave growth on several blunt cone models in AEDC Tunnel B at Mach 8 [69, 45]. The apparatus was almost identical [46, 47]. This conventional wind tunnel is well characterized [48]. The blunt-cone experiments examined the effects of the entropy layer on the hypersonic second-mode instability.

The model was a 7-degree half-angle cone with a 40-inch (1.016-m) length and a 0.15-inch (3.81 mm) nose radius. The cone angle of attack was zero, to within the accuracy with which this could be set and measured. The model was in thermal equilibrium but heat conduction within the model was not negligible. Most of the measurements were carried out at a freestream Mach number of 7.99, with a total pressure of 580 psia (4.00 MPa) and a total temperature of 1350 R (750 K).

Measurements were obtained with surface pressure taps (24) and thermocouples (32). Mean profiles were measured using pitot-pressure and total temperature probes. Instability waves were measured using calibrated constant-current hot-wire anemometry. Hot-wire spectra were recorded at one-inch (2.54-cm) intervals between 10 and 31 inches (25.4 and 78.7 cm), with additional measurements at 33, 35, and 37 inches. Four hot-wires were used for these measurements, each calibrated separately. There is no data for transition onset on the blunt cone, according to Stetson.

Growth of the first and second-mode instability waves was observed on a symmetric blunt cone under cold-flow conditions. The second-mode instability is dominant. Although amplification was only observed downstream of the nominal swallowing length, strong bluntness effects were apparent. Some entropy-layer fluctuations were also apparent, although these could not be resolved clearly and no quantitative comparisons have been attempted. Second-harmonic amplification of the second-mode waves was observed downstream, a good indication of nonlinear effects. A comparison of the second-mode amplification rate to a nonlinear computation would be interesting.

Previous Computational Comparisons

Stetson's blunt-cone flows have been computed by numerous workers. The first paper that is known to the author is Malik et al. [70], who used a Navier-Stokes code in the nose region, combined with a PNS code downstream, followed by linear instability theory. Most computations were carried out for the 0.15-inch nose radius that is described here. Malik et al. computed a peak amplification rate at $s/R_n = 175$ that was about 50% higher than the experimental value, although the frequency of peak amplification varies by only a few percent. Here, R_n is the nose radius. They speculate that the difference may be due to nonlinear effects, since a second harmonic is present there. A second comparison is shown further downstream at $s/R_n = 215$; the peak amplification rate agrees better but the shape of the curve is substantially different. A brief description of similar results is also shown in Ref. [54].

Herbert and Esfahanian et al. [71, 72] carried out a detailed comparison to the blunt-cone case. Fig. 10 in Ref. [72] shows that the actual measured wall temperatures on the cone are about 20% below adiabatic-wall values. Figs. 11 and 12 in Ref. [72] point out the lack of repeatability in the Stetson profile data, and a lack of agreement in the profile shapes. The critical importance of an accurate mean flow computation is emphasized. Fig. 15 in Ref. [71] shows computed values of the peak amplification rate at $s/R_n = 175$ that are about 70% above the experimental values, although the frequency of peak amplification agrees to within a few percent.

Kufner et al. [60, 12] carried out additional computations. Figure 2 in Ref. [60] summarizes the comparisons of all the authors; all the computations show a growth rate about 1.5 times the ex-

perimental value, at a frequency roughly 10% below the experimental value. However, these comparisons were carried out at a station 175 nose radii downstream of the tip. Figure 7b in Stetson's 1984 paper shows substantial amplification of second-harmonic frequencies at this station. Stetson believes that nonlinearity is substantial at this station, therefore a growth-rate comparison to linear theory has dubious validity. Many workers have selected this station for comparison to linear theory, following Malik et al. [70], and apparently through insufficient communication with Stetson et al. Fig. 4 in Ref. [12] shows a significant effect of the model for the second viscosity of air; however, this effect does not come near to accounting for the discrepancy with experiment. Fig. 31 in Ref. [12] shows that computations based on a second-order boundary-layer method can give good agreement with computations based on the thin-layer Navier-Stokes equations. Ref. [62] reports later computations at the Stetson blunt-cone conditions, but does not provide additional comparisons. Ref. [73] reports preliminary comparisons to the entropy-layer instability reported by Stetson et al., but not to the first or second-mode instabilities.

Mean Flow Comparisons

Surface temperature distributions are shown in Fig. 15. These were collected at the time of various mean-flow profile runs. The x locations in the legend are those of the mean-flow profiles. In the Run 101-105 series, the model appears to heat up with time. In the Run 74-76 series, smaller variations are present. Neither dataset agrees with a simple analysis of the adiabatic wall temperature.

The mean flow was measured for this experiment, but existing comparisons have uncovered some difficulties. Fig. 5 in Ref. [71] shows that an adiabatic-wall computation overpredicts the wall temperature by roughly 20%. This is thought to be due to heat transfer to the water-cooled sting support. While the measurements were carried out after thermal equilibrium was achieved, heat transfer within the model apparently cannot be neglected.

Boundary-layer profiles were also measured using pitot and total-temperature probes, as shown in Figs. 16 and 17. The total temperature plots show runs 74-76 to have uniformly thinner profiles than runs 101-104, although these are nominally repeat runs.

Unfortunately, the repeated runs reveal discrepancies of 10-15% under nominally the same conditions (see also Fig. 6 in Ref. [71]). The cause of this lack of repeatability remains uncertain. Stetson

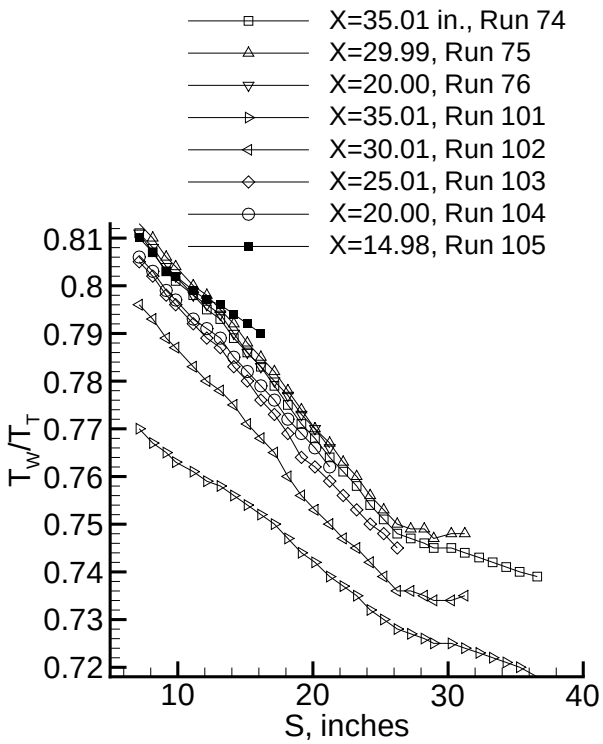

Figure 15: Wall Temperature Distributions for the Stetson Blunt Cone

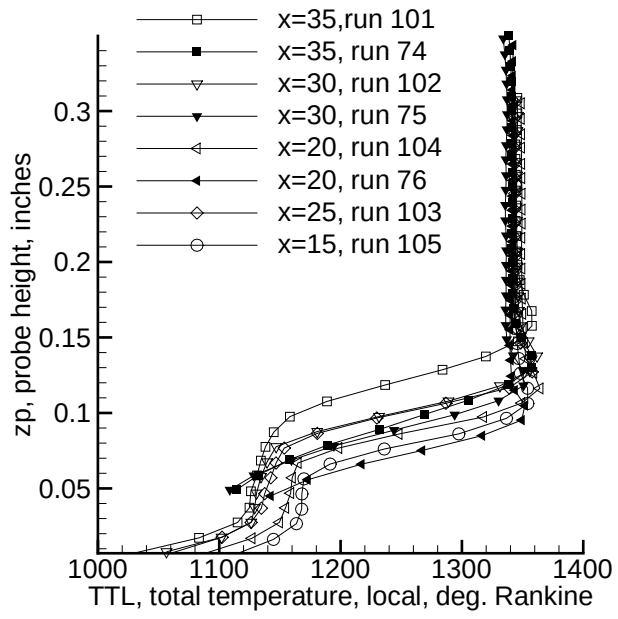

Figure 16: Mean Total Temp. Profiles for Stetson Blunt Cone

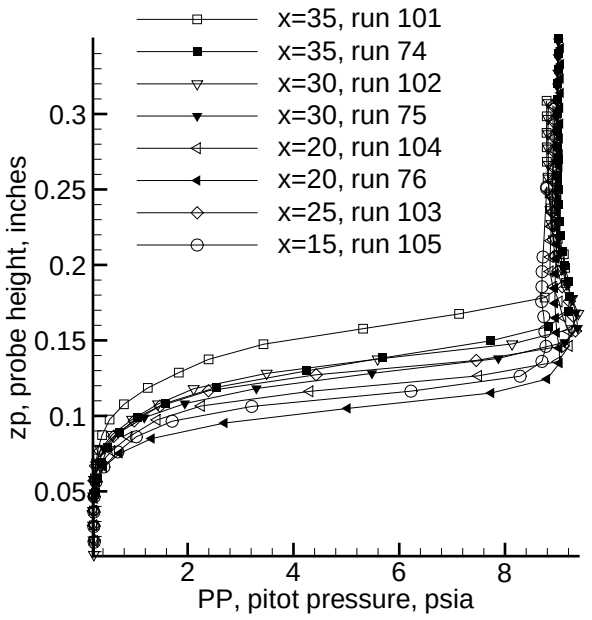

Figure 17: Mean Pitot Profiles for Stetson Blunt Cone

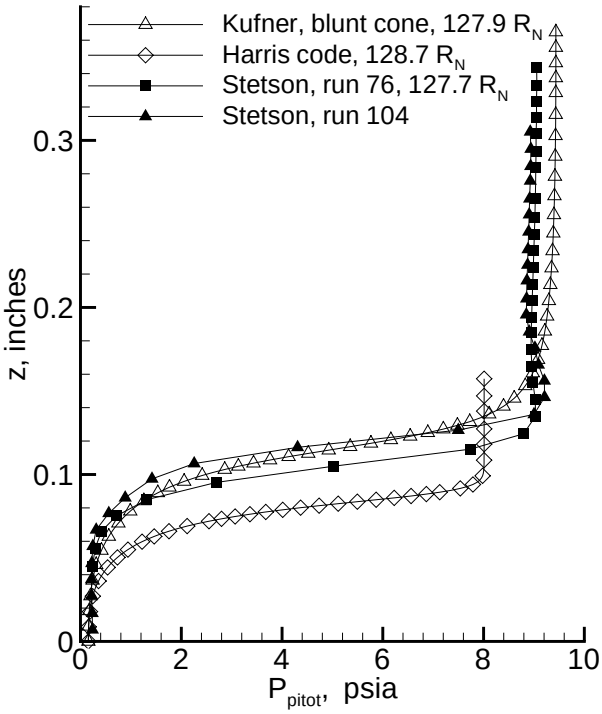

Figure 18: Comparison of Pitot Profiles for Stetson Blunt Cone

was always concerned that these profiles may also suffer from probe blockage. Boundary-layer measurements were only obtained on one ray, so detection of residual three-dimensional effects is limited to surface pressure measurements on 3 taps at 90-deg. azimuthal intervals, at two streamwise stations. Although these generally match to within the experimental error, pressure is an insensitive measure of angle of attack.

It was not possible to repeat many runs, due to the high cost of operating at AEDC. However, Stetson believes that it will be extremely difficult to obtain higher quality data in a production facility. Furthermore, budget limitations currently prohibit further tests of this type.

Fig. 18 compares the experimental data to profiles computed using the thin-layer Navier-Stokes (TLNS) equations by Kufner et al. [12], and provided by S. Hein (private communication, April 2000). The conditions are as described with Fig. 5, where the same pitot profile is shown; an adiabatic wall is assumed. The two Stetson datasets are repeat runs, obtained at the same tunnel conditions. The Harris-code computations were obtained by the present author for $T_t = 1350$R, $P_t = 580$ psia, and $M_\infty = 8.00$.

Kufner's computation shows no overshoot in the pitot profile, while overshoots are observed in both experimental profiles. Probe interference is immediately suspected, as in the sharp-cone case. Although the Kufner computations give fair agreement for the boundary-layer thickness, the Harris-code computations show poor agreement for both the edge pitot pressure and the boundary-layer thickness.

The limitations of the first-order boundary-layer theory are thought to cause the problems with the Harris-code results. The Harris code uses a variable `VELEDG` to define the edge of the boundary-layer as a fraction of the inviscid edge velocity. This parameter was changed to 99% from the usual value of 99.99% (which was used in order to get many grid points near the boundary-layer edge for the stability analysis). Fig. 19 shows the results for the same conditions as in Fig. 18, again at $s = 128.7R_N$. The edge pitot pressure decreases by 20%, causing the profiles to be even farther away from the experiment and the more-accurate Kufner computation. This effect must be related to the way that the first-order boundary-layer approach obtains the edge conditions by tracing streamlines from the curved bow shock. The use of a first-order boundary-layer method for computation of the blunt-cone profile is clearly inadequate for stability purposes.

Fig. 20 compares total-temperature profiles

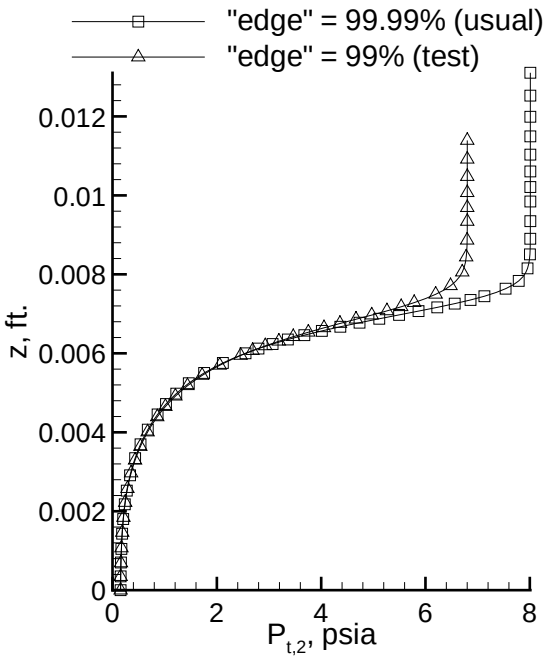

Figure 19: Effect of Boundary-Layer Edge Parameter on Harris-Code Profile

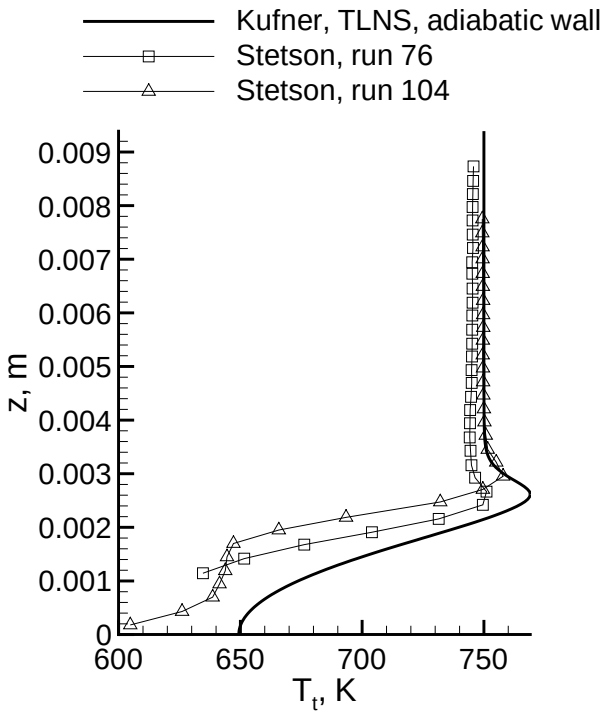

Figure 20: Comparison of Total-Temperature Profiles for Stetson Blunt Cone

from the same Kufner computation to the Stetson profiles from two repeat runs. The Stetson profiles were obtained at $s = 127.7R_N$, and the Kufner profile is from $s = 127.9R_N$. Here, the three profiles are qualitatively similar, as all contain similar overshoots near the boundary-layer edge. However, the quantitative agreement is poor. The poor agreement is particularly critical when one remembers that the stability computations are highly sensitive to the second derivatives of the profiles. Since Stetson's total-temperature measurements were obtained at the same time as the pitot measurements, using a single rather large rake, both pitot and total-temperature measurements may be contaminated by probe interference. Also, the repeatability of the measurements is only about 15%. While the TLNS analysis may be accurate enough for stability purposes, the quality of the experimental data is insufficient to validate the computation.

Instability-Wave Comparisons

AEDC carried out spectral analyses of the hot-wire data and produced tables of amplitude vs. frequency at these streamwise stations. Tabulated data is available both for the uncalibrated voltage spectra *and* for calibrated spectra reported for total temperature and massflux. These printed tables were made available by Roger Kimmel, and have been entered into electronic form. Figure 21 shows the massflow spectra. Figure 22 shows the total temperature spectra. The spectra are again normalized by the mean value at the hot-wire location, given by the streamwise arclength s and the probe height `ZA`. The signal-to-noise ratio is larger for the total temperature spectra, since the constant-current hot wire was operated at low overheat.

Rosenboom et al. computed second-mode N-factors for this case [62], using an accurate Thin-Layer Navier-Stokes mean flow. The instabilities were computed using linear local and nonlocal methods. Hein provided the tabulated local-method N factors from Fig. 17 of Ref. [62] (private communication, August 2000). These data are replotted in Fig. 23, and compared to second-mode N factors computed by the present author using the Harris-code boundary-layer profiles and the e^{Malik} code. While the 110 and 120 kHz results are not too far apart, the N factors for the higher frequencies differ by a factor of more than 2. Both computations were carried out for $T_t = 1350$R or 750K, $M_\infty = 8.00$, and $R_N = 0.15$ in. or 3.81 mm. The present computation uses $P_t = 580$ psia and the Sutherland viscosity law, while Rosenboom et al. used $Re_\infty = 8.202 \times 10^6$/m, which is obtained

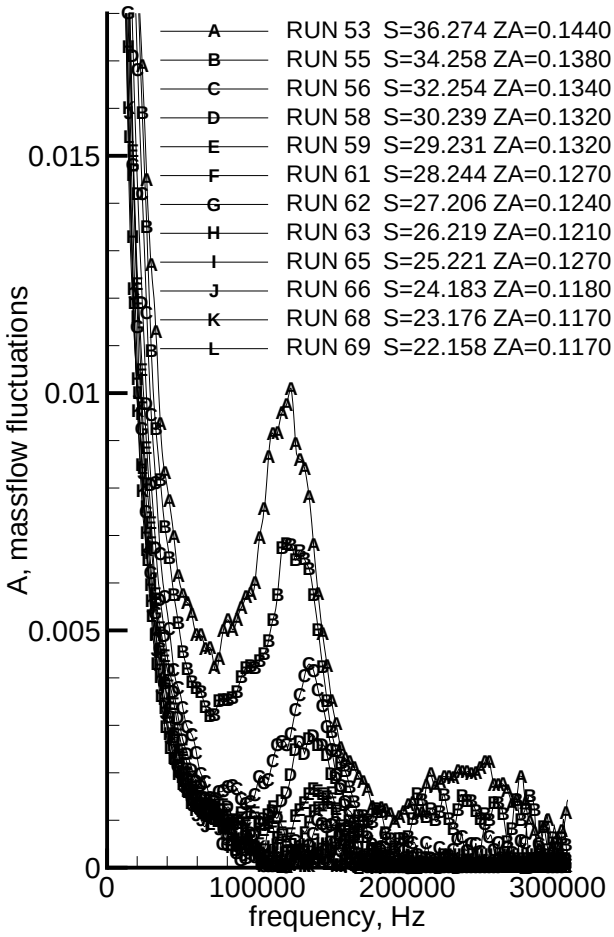

Figure 21: Massflux Spectra for Stetson Blunt Cone

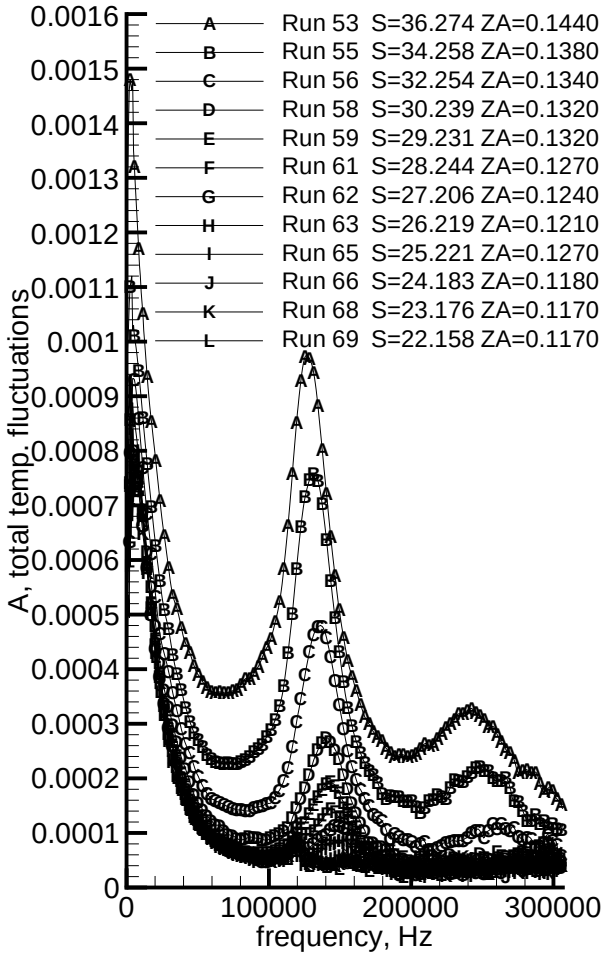

Figure 22: Total Temperature Spectra for Stetson Blunt Cone

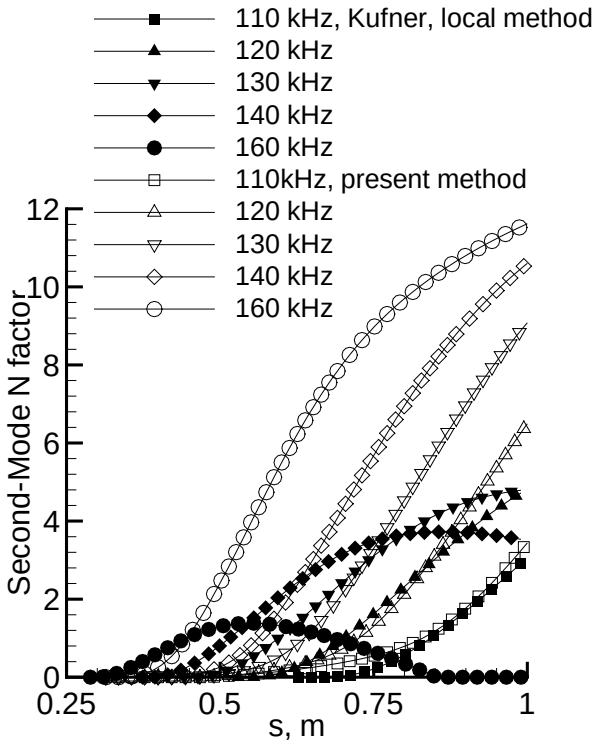

Figure 23: N factors for Blunt Cone Using Two Methods

from this same total pressure by using the Mack-modified form of the Sutherland law. If the normal Sutherland law is used, $Re_\infty = 8.76 \times 10^6$/m, which is only 7% higher and insufficient to explain the discrepancy. The substantial errors in the mean-flow profiles caused by the use of the first-order boundary-layer code result in very large errors in the highly-sensitive instability computation. First-order boundary-layer methods are inadequate for computation of blunt-cone instabilities, even for preliminary design purposes.

Finally, the Kufner N-factors shown in Fig. 23 were used to compute amplification ratios, and compared to the Stetson amplification ratios for total temperature. The total temperature data was selected since the signal-to-noise ratio appears better. Run 56 at $s = 32.254$ in. was chosen as the terminal station for a linear comparison, since Fig. 22 shows that the (nonlinear) second harmonic becomes significant further downstream. Run 59 at $s = 29.231$ in. was chosen as the reference location, since this is the furthest upstream location for which the amplified frequencies rise clearly above the background noise. This again delineates a small linear-amplification region, as for the sharp cone, probably again due to signal-to-noise issues. The amplification ratios from Run 56 to Runs 58 and 59 were computed, and compared to values that were linearly interpolated from the Kufner data of Fig. 23. Fig. 24 shows the results. Both methods show a small amplification of about 1.4 or 1.5 to $S = 30.239$ in., and both show a larger amplification of 2.9 to 3.3 to $S = 32.254$. The most amplified frequencies differ by perhaps 10% and the largest amplification factors differ by perhaps 10% also. Outside the range of computational amplification, the experimental amplification factors are generally not reliable, due to signal-to-noise problems. While the figure again shows general agreement, it is still clearly insufficient for reliable code validation. Better experimental data is needed.

Summary

Profiles produced by a first-order boundary-layer method are clearly insufficient for stability analyses, although second-order boundary-layer techniques do appear to be sufficient. Good agreement between computation and experiment remains to be obtained. Since an accurate comparison of the mean flow profiles is not possible, due to probe interference, new experiments will almost certainly be needed to resolve the disagreement.

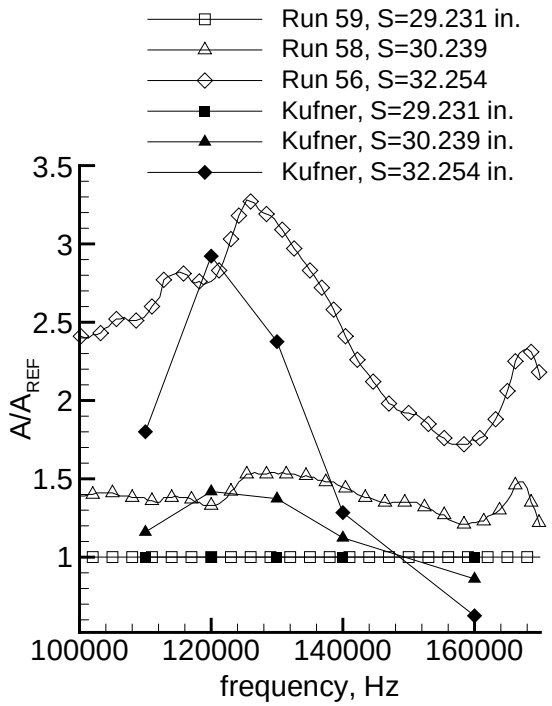

Figure 24: Amplification Ratios for Blunt Cone

Sharp Flared Cone at Mach 6

Three instability experiments were carried out in the NASA Langley Mach-6 quiet tunnel before it was decommissioned [74]. Comparisons between experimental and computational N-factors are shown for all three experiments in Fig. 11 of Ref. [74]; good agreement was obtained. Due to schedule limitations, only one of the three was able to obtain calibrated mean-flow profiles [75, 76, 77]. All measurements were made using natural fluctuations, without controlled disturbance generators. All experiments were carried out with constant-voltage anemometry (CVA), due to electromagnetic noise problems with more conventional anemometers. No systematic studies of CVA calibration techniques had been carried out at that time, so the calibrations are limited. The experiments were carried out on both sharp and blunt cones, but extensive data is available only for the sharp cone.

The model was a 50.8-cm sharp cone. The first 25.4 cm formed a straight cone with a 5-deg. half-angle. This was followed by a gentle flare with a 2.364-m radius of curvature. The profile shape is continuous; only the second derivative is discontinuous at the match point. The tip had a nominal radius of 2.5 microns. The cone angle of attack was nearly zero; however, most measurements were carried out at a yaw angle of approximately 0.1 deg. and a pitch angle of approximately 0.1 deg. [77, p. 20]. Appendix D of Ref. [77] reports additional measurements carried out after additional efforts were made to align the model at zero angle of attack.

The measurements were carried out at Mach 5.91, with a total pressure of 896 kPa and a total temperature of 450K. The freestream Reynolds number was 9.25×10^6/m (note the typographical error on p. 2497 of Ref. [76]).

Measurements were obtained with surface pressure taps (29) and thermocouples (51). Mean flow profiles were measured using hot wires and CVA. Fluctuating profiles were obtained using the same hot wires, but no calibrated fluctuations were reported. Thus, no calibrated eigenfunctions are available.

These data were also obtained under equilibrium-wall temperature conditions. That is, the measurements were obtained only after the model-wall thermocouples reached steady-state temperatures. This occurred approximately 15-20 minutes after initiation of Mach-6 flow, following a subsonic preheat. Unfortunately, as for the Stetson data, this is not the same as adiabatic-wall conditions, for Chokani states that the heat-transfer within the model is not negligible.

Growth of first and second-mode instability waves was observed on an axisymmetric cone under cold-flow conditions, in a quiet tunnel [78]. An adverse pressure gradient exists on the rear half of the model. Second-mode amplification is observed. Görtler interactions are possible on the concave flare, although no experimental evidence is available.

Lachowicz et al. report agreement of 2-5% with linear-instabilty N-factor computations for the second-mode wave growth [76, Fig. 9]. However, the ratio of CVA fluctuating voltages was taken as the ratio of wave amplitude. This assumption was used by Stetson and others for constant-current or constant-temperature anemometry, when the measurements were carried out with the hot wire at identical mean-flow conditions. However, the validity of this assumption for the Lachowicz CVA data is presently being reviewed.

If this assumption can be verified, and any errors caused by it can be quantified, this dataset may be the best of the three. Although the aft end of the cone was outside of the fully quiet region, this is the only data obtained under quiet conditions. Static pressure data was obtained at 3 azimuthal positions to check angle of attack, although all boundary-layer

measurements were again obtained on only one ray. The mean flow profiles are in fairly good agreement with existing computations.

Additional computations have now been carried out (Ref. [79] and [80]). However, the experimental data are not yet available in tabulated form; detailed comparisons may be carried out at a later date. New computations were reported in Ref. [65], but wave amplifications have not yet been compared.

Summary

Accurate agreement between computation and experiment remains to be achieved even for linear instability on a sharp cone.

The boundary-layer profiles obtained during the Stetson cone experiments suffer from probe interference and are also repeatable only to 15%. The quality of these profiles is insufficient for code validation. On both the sharp and blunt cones, the second-mode waves amplify by less than a factor of 4 within the linear region, after achieving a significant signal-to-noise ratio. This is insufficient for reliable code validation. Conventional tunnel experiments will require controlled perturbations to achieve substantial linear amplifications that would allow an accurate validation of linear computations. It is expected that a linear validation will usually be needed before a nonlinear computation can then be validated.

First-order boundary-layer methods are inadequate for computation of blunt-cone instabilities, even for preliminary design purposes.

Acknowledgements

The present analysis is part of a new experimental and computational study of blunt-cone transition that is funded by Sandia National Laboratory under Contract BG-7114. The technical liason is Dr. Dave Kuntz. Sandia provided the inviscid blunt-cone solutions, through Kuntz. Roger Kimmel from the Air Force Research Laboratory in Dayton provided many pages of tabulated printout for the Stetson experiments, along with much other critical information. Discussions with Kimmel and Ken Stetson (retired from AFRL) were critical to interpretation of this data. Jocelyn Muhl and Novi Sutanto entered the tabulated Stetson data into electronic form with excellent accuracy. Stefan Hein from the DLR in Göttingen, Germany, was extremely helpful. In particular, Hein provided tabulated electronic results from the computations of the Dallmann group, and postprocessed some of the Göttingen results to obtain pitot profiles.

Discussions with the members of NATO RTO WG-10 have also been helpful; these members include Daniel Arnal of ONERA, Toulouse, France, Eli Reshotko of Case Western University, Cleveland, Ohio, Graham Candler of the Univ. of Minnesota, USA, Roger Kimmel of AFRL, and Anatoly Maslov of ITAM, Novosibirsk, Russia.

References

[1] Eli Reshotko. Boundary layer instability, transition, and control. Paper 94-0001, AIAA, January 1994. The 1994 Dryden Lecture in Research.

[2] Tony C. Lin, Wallis R. Grabowsky, and Kevin E. Yelmgren. The search for optimum configurations for re-entry vehicles. *J. of Spacecraft and Rockets*, 21(2):142–149, March-April 1984.

[3] Jiayu Niu, Guobin Xu, Rongda Cao, and Aimin Ren. Study of the wake flow field and the radar cross section of a reentry vehicle. *Acta Aerodynamica Sinica*, 14(4):422–429, December 1996.

[4] D. M. Bushnell. Notes on initial disturbance fields for the transition problem. In M. Y. Hussaini and R.G. Voigt, editors, *Instability and Transition, Volume I*, pages 217–232, Berlin, 1990. Springer-Verlag. Materials of the workshop held May 15 – June 9,1989 in Hampton, Virginia.

[5] William S. Saric. Görtler vortices. *Annual Review of Fluid Mechanics*, 26:379–409, 1994.

[6] L. M. Mack. Boundary layer linear stability theory. In *Report 709, Special Course on Stability and Transition of Laminar Flow*, pages 1–81. AGARD, March 1984.

[7] H.L. Reed and W.S. Saric. Stability of three-dimensional boundary layers. *Annual Review of Fluid Mechanics*, 21:235–284, 1989.

[8] Th. Herbert. Secondary instability of boundary layers. *Annual Reviews of Fluid Mechanics*, 20:487–526, 1988.

[9] R. Narasimha. The laminar-turbulent transition zone in the turbulent boundary layer. *Progress in Aerospace Science*, 22:29–80, 1985.

[10] Steven P. Schneider. Flight data for boundary-layer transition at hypersonic and supersonic speeds. *Journal of Spacecraft and Rockets*, 36(1):8–20, 1999.

[11] Mujeeb R. Malik. Prediction and control of transition in supersonic and hypersonic boundary layers. *AIAA Journal*, 27(11):1487–1493, November 1989.

[12] E. Kufner, U. Dallmann, and J. Stilla. Instability of hypersonic flow past blunt cones – effects of mean flow variations. Paper 93-2983, AIAA, July 1993.

[13] Geza Schrauf, Jean Perraud, Domenico Vitiello, and Fung Lam. A comparison of linear stability theories using F100-flight tests. Paper 97-2311, AIAA, June 1997.

[14] L. Kleiser and T. Zang. Numerical simulation of transition in wall-bounded shear flows. *Annual Reviews of Fluid Mechanics*, 23:495–537, 1991.

[15] Th. Herbert. Parabolized stability equations. *Ann. Rev. Fluid Mech.*, 29:245–284, 1997.

[16] Thorwald Herbert. On the stability of 3D boundary layers. Paper 97-1961, AIAA, June 1997.

[17] Sean H. Hu and Xiaolin Zhong. Hypersonic boundary-layer stability over blunt leading edges with bow-shock effects. Paper 98-0433, AIAA, January 1998.

[18] C.-L. Chang, H. Vinh, and M.R. Malik. Hypersonic boundary-layer stability with chemical reactions using PSE. Paper 97-2012, AIAA, June 1997.

[19] Mary L. Hudson, Ndaona Chokani, and Graham V. Candler. Linear stability of hypersonic flow in thermochemical equilibrium. *AIAA Journal*, 35(6):958–964, 1997.

[20] I.E. Beckwith and C.G. Miller III. Aerothermodynamics and transition in high-speed wind tunnels at NASA Langley. *Annual Review of Fluid Mechanics*, 22:419–439, 1990.

[21] Steven P. Schneider. Effects of high-speed tunnel noise on laminar-turbulent transition. Paper 2000-2205, AIAA, June 2000.

[22] H.H. Hamilton II, D.R. Millman, and R.B. Greendyke. Finite-difference solution for laminar or turbulent boundary layer flow over axisymmetric bodies with ideal gas, CF4, or equilibrium air chemistry. Technical Paper 3271, NASA, December 1992.

[23] Christopher J. Roy and Frederick G. Blottner. Assessment of one- and two-equation turbulence models for hypersonic transitional flows. Paper 2000-0132, AIAA, January 2000.

[24] Kenneth F. Stetson. Hypersonic transition testing in wind tunnels. In M. Y. Hussaini and R.G. Voigt, editors, *Instability and Transition, Volume I*, pages 91–97, Berlin, 1990. Springer-Verlag.

[25] Y.S. Kachanov and A. Michalke. Three-dimensional instability of flat-plate boundary layers: theory and experiment. *European J. of Mechanics B/Fluids*, 13(4):401–422, 1994.

[26] H.L. Reed, T.S. Haynes, and W.S. Saric. CFD validation issues in transition modelling. *AIAA Journal*, 36(5):742–751, May 1998.

[27] D. P. Aeschliman and W. L. Oberkampf. Experimental methodology for computational fluid dynamics code validation. *AIAA Journal*, 36(5):733–741, May 1998.

[28] Christopher J. Roy, Mary A. McWherter Payne, and William Oberkampf. Verification and validation for laminar hypersonic flowfields. Paper 2000-2550, AIAA, June 2000.

[29] Eli Reshotko. A program for transition research. *AIAA Journal*, 13(3):261–265, March 1975.

[30] D.A. Bountin, A.N. Shiplyuk, and A.A. Sidorenko. Experimental investigations of disturbance development in the hypersonic boundary layer on a conical model. In H. Fasel and W. Saric, editors, *Laminar-Turbulent Transition. Proceedings of the IUTAM Symposium, Sedona, 1999*, pages 475–480, Berlin, 2000. Springer-Verlag.

[31] J. Daywitt, D. Brant, and F. Bosworth. Computational technique for three-dimensional inviscid flow fields about reentry vehicles. Technical report, General Electric Company, Philadelphia, Pennsylvania, April 1978.

[32] R.W. Noack and A.R. Lopez. Inviscid flow field analysis of complex reentry vehicles: Volume I, description of numerical methods, Volume II, users manual. Technical Report SAND87-0776, Sandia National Laboratories, Albuquerque, New Mexico, October-November 1988.

[33] J. E. Daywitt, D. Brant, and F. Bosworth. Computational technique for three-dimensional inviscid flow fields about reentry vehicles. Technical Report TR-79-5, SAMSO, April 1978.

[34] J. E. Daywitt, M. Wade, D. J. Szostowski, and S. Yalisove. Split-coefficient matrix form of the GE-RSD three-dimensional inviscid supersonic flow field code (3IS/SCM). Technical Report 82SDR2029, General Electric Company, Philadelphia, Pennsylvania, April 1982.

[35] J. E. Daywitt, D. J. Szostowski, and D. A. Anderson. A split-coefficient/locally monotonic scheme for multishocked supersonic flow. *AIAA Journal*, 21(6):871–880, June 1983.

[36] R. F. Warming and R. M. Beam. Upwind second-order difference schemes and applications in aerodynamic flows. *AIAA Journal*, 14:1241–1249, September 1976.

[37] B. Van Leer. Flux vector splitting for the Euler equations. *Lecture Notes in Physics*, 170:507–512, 1982.

[38] J.E. Harris and D.K. Blanchard. Computer program for solving laminar, transitional, or turbulent compressible boundary-layer equations for two-dimensional and axisymmetric flow. Technical Report NASA-TM-83207, NASA, February 1982.

[39] R.N. Gupta, K.P. Lee, E.V. Zoby, J.N. Moss, and R.A. Thompson. Hypersonic viscous shock-layer solutions over long slender bodies – Part I: high Reynolds number flows. *J. Spacecraft*, 27(2):175–184, March-April 1990.

[40] Kam-Pui Lee and Roop N. Gupta. Viscous-shock-layer analysis of hypersonic flows over long slender vehicles. Contractor Report CR-189614, NASA, March 1992.

[41] Mujeeb R. Malik. e**Malik: A new spatial stability analysis program for transition prediction using the e**N method. Technical Report HTC-8902, High Technology Corporation, March 1989. See also HTC-9203, which is almost identical.

[42] M.R. Malik. Numerical methods for hypersonic boundary layer stability. *Journal of Computational Physics*, 86:376–413, 1990.

[43] Steven P. Schneider. Design of a Mach-6 quiet-flow wind-tunnel nozzle using the e**N method for transition estimation. Paper 98-0547, AIAA, January 1998.

[44] K.F. Stetson, E.R. Thompson, J.C. Donaldson, and L.G. Siler. Laminar boundary layer stability experiments on a cone at Mach 8, part 1: Sharp cone. Paper 83-1761, AIAA, June 1983.

[45] K. Stetson and R. Kimmel. On hypersonic boundary-layer stability. Paper 92-0737, AIAA, January 1992.

[46] L.G. Siler and J.C. Donaldson. Boundary layer measurements on slender blunt cones at free-stream Mach number 8. Technical Report AEDC-TSR-79-V71, AEDC, December 1979.

[47] D.B. Carver, L.G. Siler, and J.C. Donaldson. Boundary layer measurements on slender blunt cones at Mach number 8 – Part II. Technical Report AEDC-TSR-80-V36, AEDC, July 1980.

[48] J. Donaldson and S. Coulter. A review of free-stream flow fluctuation and steady-state flow quality measurements in the AEDC/VKF supersonic tunnel A and hypersonic tunnel B. Paper 95-6137, AIAA, April 1995.

[49] L. M. Mack. Boundary-layer stability analysis for sharp cones at zero angle-of-attack. Technical Report AFWAL-TR-86-3022, Air Force Wright Aeronautical Laboratories, August 1986.

[50] L. M. Mack. Stability of axisymmetric boundary layers on sharp cones at hypersonic Mach numbers. Paper 87-1413, AIAA, June 1987.

[51] J. Kendall. Wind tunnel experiments relating to supersonic and hypersonic boundary-layer transition. *AIAA Journal*, 13:290–299, 1975.

[52] A. Demetriades. Laminar boundary layer stability measurements at Mach 7 including wall temperature effects. Technical Report AFOSR-TR-77-1311, AFOSR, November 1977.

[53] C.-L. Chang, M. R. Malik, and M.Y. Hussaini. Effects of shock on the stability of hypersonic boundary layers. Paper 90-1448, AIAA, June 1990.

[54] M. Malik, T. Zang, and D. Bushnell. Boundary layer transition in hypersonic flows. Paper 90-5232, AIAA, October 1990.

[55] C.-L. Chang and M. R. Malik. Non-parallel stability of compressible boundary layers. Paper 93-2912, AIAA, July 1993.

[56] Martin Simen and Uwe Dallmann. On the instability of hypersonic flow past a pointed cone – comparison of theoretical and experimental results at Mach 8. Technical Report DLR-Forschungsbericht DLR-FB-92-02, Deutsche Forschungsanstalt für Luft- und Raumfahrt, Göttingen, Germany, August 1991. In English.

[57] Martin Simen and Uwe Dallmann. On the instability of hypersonic flow past a pointed cone – comparison of theoretical and experimental results at Mach 8. In *Theoretical and experimental methods in hypersonic flows*. AGARD, May 1992. Paper 31 in CP-514.

[58] M. Simen and U. Dallmann. Nonlocal vs. local instability of compressible flows including body metric, flow divergence, and 3D-wave propagation. Paper 93-2982, AIAA, July 1993.

[59] Ewald Kufner. Numerische Untersuchungen der Strömungsinstabilitäten an spitzen und stumpfen Kegeln bei hypersonischen Machzahlen. Technical Report DLR-Forschungsbericht 95-11, Deutsche Forschungsanstalt für Luft- und Raumfahrt, Göttingen, Germany, February 1995. In German.

[60] E. Kufner and U. Dallmann. Entropy- and boundary layer instability of hypersonic cone flows – effects of mean flow variations. In R. Kobayashi, editor, *Laminar-Turbulent Transition*, pages 197–204, Berlin, 1995. Springer-Verlag. Proceedings of the IUTAM Symposium held in Sendai, Japan, September 1994.

[61] Joseph W. Cleary. Effects of angle of attack and nose bluntness on the hypersonic flow past cones. Paper 66-414, AIAA, June 1966.

[62] I. Rosenboom, S. Hein, and U. Dallmann. Influence of nose bluntness on boundary-layer instabilities in hypersonic cone flows. Paper 99-3591, AIAA, June 1999.

[63] James M. Kendall, Jr. An experimental investigation of leading-edge shock-wave–boundary-layer interaction at Mach 5.8. *J. Aero. Sci.*, 24:47–56, January 1957.

[64] M. V. Morkovin and W.S. Bradfield. Probe interference in measurements in supersonic laminar boundary layers. *Journal of the Aeronautical Sciences*, 21(11):785–787, November 1954.

[65] M.L. Manning and N. Chokani. PSE analysis of a quiet tunnel hypersonic boundary layer flow. Paper 2000-2652, AIAA, June 2000.

[66] Steven P. Schneider. Development of quiet-flow supersonic wind tunnels for laminar-turbulent transition research. Contractor Report CR-197286, NASA, January 1995.

[67] M.J. Zucrow and J.D. Hoffman. *Gas Dynamics, Volume II: Multidimensional Flow*. Robert Krieger, Malabar, Florida, 1985.

[68] Dale W. Ladoon and Steven P. Schneider. Measurements of controlled wave packets at Mach 4 on a cone at angle of attack. Paper 98-0436, AIAA, January 1998.

[69] K.F. Stetson, E.R. Thompson, J.C. Donaldson, and L.G. Siler. Laminar boundary layer stability experiments on a cone at Mach 8, part 2: Blunt cone. Paper 84-0006, AIAA, January 1984.

[70] M.R. Malik, R.E. Spall, and C.-L. Chang. Effect of nose bluntness on boundary layer stability and transition. Paper 90-0112, AIAA, January 1990.

[71] T. Herbert and V. Esfahanian. Stability of hypersonic flow over a blunt body. In *Theoretical and Experimental Methods in Hypersonic Flows*, May 1992. Paper 28 in AGARD CP-514.

[72] V. Esfahanian, Th. Herbert, and O.R. Burggraf. Computation of laminar flow over a long slender axisymmetric blunted cone in hypersonic flow. Paper 92-0756, AIAA, January 1992.

[73] G. Dietz and S. Hein. Entropy-layer instabilities over a blunted flat plate in supersonic flow. *Physics of Fluids*, 11(1):7–9, January 1999.

[74] Stephen P. Wilkinson. A review of hypersonic boundary layer stability experiments in a quiet

Mach 6 wind tunnel. Paper 97-1819, AIAA, June 1997.

[75] J.T. Lachowicz, N. Chokani, and S.P. Wilkinson. Hypersonic boundary layer stability over a flared cone in a quiet tunnel. Paper 96-0782, AIAA, January 1996.

[76] J.T. Lachowicz, N. Chokani, and S. P. Wilkinson. Boundary-layer stability measurements in a hypersonic quiet tunnel. *AIAA Journal*, 34(12):2496–2500, December 1996.

[77] J.T. Lachowicz and N. Chokani. Hypersonic boundary layer stability experiments in a quiet wind tunnel with bluntness effects. Technical Report CR-198272, NASA, January 1996. Identical to Lachowicz's PhD thesis.

[78] Alan E. Blanchard, Jason T. Lachowicz, and Stephen P. Wilkinson. NASA Langley Mach 6 quiet wind-tunnel performance. *AIAA Journal*, 35(1):23–28, January 1997.

[79] P. Balakumar and M.R. Malik. Effect of adverse pressure gradient and wall cooling on instability of hypersonic boundary layers. Technical Report HTC-9404, High Technology Corporation, March 1994.

[80] C. D. Pruett and C.-L. Chang. Direct numerical simulation of hypersonic boundary-layer flow on a flared cone. *Theoret. Comput. Fluid Dynamics*, 11(1):49–67, March 1998.